Assessment of H-Darrieus Hydrokinetic Turbines by Configuration with a Blocking Plate Using a Design of Experiment Approach

Angie Guevara Muñoz[1]*, M. A. Rodriguez-Cabal[1], Diego Hincapie Zuluaga[2]

[1] Department of Mechatronics and Electromechanics, Instituto Tecnologico Metropolitano, Medellín 050036, Colombia
[2] Department of Mechanical Engineering, University of Antioquia, Medellín 050010, Colombia

Corresponding Author Email: angieguevara220191@correo.itm.edu.co

ABSTRACT

The use of H-Darrieus Hydrokinetic Turbines (HDHTs) is a viable alternative to small hydropower plants. They are recognized for their low environmental impact since they operate without requiring water dams, though they have limited automatic start-up capability. However, through the proper configuration or external accessories, they can increase or decrease their performance because of the blade velocity and pressure. The objective of this study is to evaluate and compare the moment coefficient and power coefficient generated by two configurations of H-Darrieus turbines using DoE-ANOVA and CFD simulations to obtain experimental solutions. The simulation was performed in 2D in a transient state. The DoE-ANOVA results show that the factors of solidity and blocking plate position are significant and directly affect the turbine performance, showing that the most significant factor is solidity. In addition, it was found that the best configuration is solidity 1.35 with case C (blocking plate at 0.665 m), similarly, it produces an improvement of the maximum and minimum moment coefficient of 10.6% and 20% respectively compared to the base case (case A).

1. INTRODUCTION

Due to the high global energy demand and the environmental awareness that has been acquired over the years. The study of renewable energies plays a very important role in society and its accelerated development leads to the expectation that hydro power will account for 16% of global electricity production by 2025, according to the International Energy Agency (IEA) [1]. In Latin American countries like Colombia, the great diversity of their natural resources has allowed them to obtain energy from renewable sources, mainly from hydroelectric plants due to their high power, efficiency, cleanliness and lower generation costs [2]. Nevertheless, in Third World countries there are isolated geographical areas where a difficult access prevents the coverage of the national electricity system, which means that not all people have electricity supply [3]. Due to this situation, some communities have chosen to use renewable energy such as Small Hydroelectric Power Plants (HPP) [4] that need less construction space, lower cost and are a source of energy capable of protecting the environment [5]. Within the HPP are the H-Darrieus turbines, which are hydraulic systems that operate with the natural current of the river, are economical and do not require considerable civil works for their construction [6, 7]. However, hydrokynetic turbines presents challenges in their design due to the fact that each installation site requires a different design focused on the type and size of the blades, and the turbine radius. And the fact that in some rivers it is not possible to obtain adequate operating flow velocities, it is necessary to make adjustments to improve the harnessing of energy.

H-Darrieus Hydrokinetic Turbines (HDHTs) are composed of three primary elements: the central shaft, the support arms, and the blades. The central shaft transmits the kinetic energy harvested from the fluid to an electric generator, while the support arms hold the blades, which are activated by their interaction with the fluid. This interaction is influenced by the geometric characteristics of the blades positioned on the periphery [8]. Solidity, a key parameter that determines the HDHTs' geometry, greatly affects their behavior [9, 10]. For instance, turbines with low solidity exhibit better self-starting capabilities [11]. Additionally, increasing solidity shifts and narrows the maximum efficiency point on the Power Coefficient (C_p) vs Tip Speed Ratio (TSR) curve [12]. These turbines generally have low self-starting capacity, prompting various authors to evaluate numerically and experimentally with external accessories like plates, blades, or diffusers to enhance efficiency, self-starting capacity [13], and reduce negative momentum [14-17]. For example, Gosselin et al. [18] in found that blade configurations with end plates limit efficiency losses. Moreover, Patel et al. [19] conducted an experimental study on a HDHT with a blocking plate configuration, concluding that this setup directly impacts performance.

To make a correct design of a HDHT, various numerical studies must be realized, departing from the analysis of the zone where it will be installed, made the analysis to prove different characteristics to find the most efficient configuration

and dimensions of the turbine. This design process is commonly developed in simulation spaces where exists a high computational cost due to the complexity of the geometry and the multiples items which are related to that. The Design of Experiment has gained popularity in recent years due to its ability to significantly reduce the number of simulations required to identify the optimal solution. Such is the case presented by Rueda-Bayona et al. [20], where the Design of Experiment (DoE) and Analysis of Variance (ANOVA) methods were conducted to optimize a hydrokinetic turbine for low velocity conditions. To validate and construct the data, Computational Fluid Dynamics (CFD) simulations were carried out to evaluate each condition. On the other hand, specialized literature studies can be found where the DoE analysis is implemented for other types of turbines such as Francis turbine [21], and variable geometry turbocharger [22] where the importance of the design of experiments as a valuable tool to minimize the number of experiments to found an adequate solution is highlighted.

It is for the above that in this paper a general DoE-ANOVA is carried out, to analyze the impact of solidity and the use of a blocking plate. Using two different solidities (1.35 and 1.79) and the blocking plate at two different distances. To validate the methodology implemented CFD simulations were used and the addition of a case base as reported by Patel et al. [19], where the two different H-Darrieus rotors are modeled with symmetric NACA 0018 profiles. The null hypothesis planted for this study is that the change of solidity and the addition of a blocking plate does not improve the power coefficient. The objective of this work is to demonstrate that by means of the use of a Design of Experiment along with CFD simulation, it is possible to evaluate the performance of hydrokinetic turbines with a reduction in the computational cost, due to the reduction of analysis points, which reduces the amount of simulations that must be performed to obtain an adequate solution to the design problems of this type of turbines.

2. METHODOLOGY

2.1 Theoretical framework

Available kinetic energy P_T in the water is estimated using Eq. (1) [23]:

$$P_T = \frac{1}{2}\rho A U^3 \tag{1}$$

where, ρ is the density, A is the projected rotor area, and U represents the free flow velocity. As the turbines do not have the capacity to extract all the available energy from the water, it is necessary to consider the power coefficient C_P, to estimate the power that is extracted by the shaft in an interval of a water current that passes through the cross-section A of the rotor [24], as shown in Eq. (2).

$$P_{extracted} = C_P\left(\frac{1}{2}\rho A U^3\right) \tag{2}$$

Solving C_P from Eqs. (1) and (2) gives the power coefficient as:

$$C_P = \frac{P_T}{\frac{1}{2}\rho A U^3} \tag{3}$$

where, P_T is the mechanical power, where M is the momentum and ω the angular velocity of the turbine shaft. Additionally, the moment coefficient C_m is the amount of mechanical energy that can be obtained from the turbine per unit of kinetic energy of the water passing through it.

$$C_M = \frac{M}{\frac{1}{2}\rho A U^2} \tag{4}$$

Another dimensionless parameter is the solidity σ which describes the relationship between the front surface of the blades and the surface of the rotor disk. Eq. (5). shows its definition, where N is the number of blades, c is the chord length and R is the radius of rotation of the turbine.

$$\sigma = \frac{Nc}{R} \tag{5}$$

2.2 Design of experiment and control surface

For the testing development, DoE: General Full Factorial Design was proposed, where an ANOVA analysis method was implemented. ANOVA allows for the statistical analysis of how independent variables affect a dependent variable. The DoE was conducted with two factors: solidity and position of the blocking plate. Where each factor was tested at two and three levels, respectively. The experiment was carried out with a repetition.

Note: Authors' own source
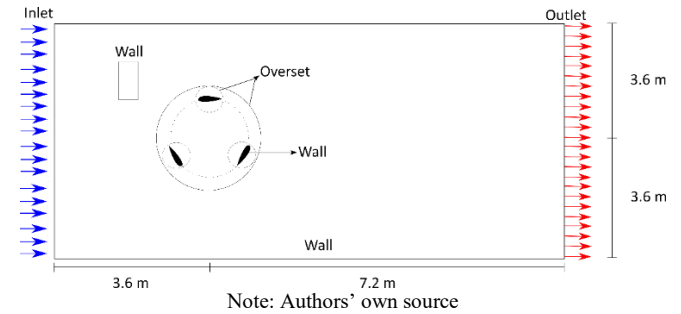
Figure 1. Schematic view of domains and boundary conditions
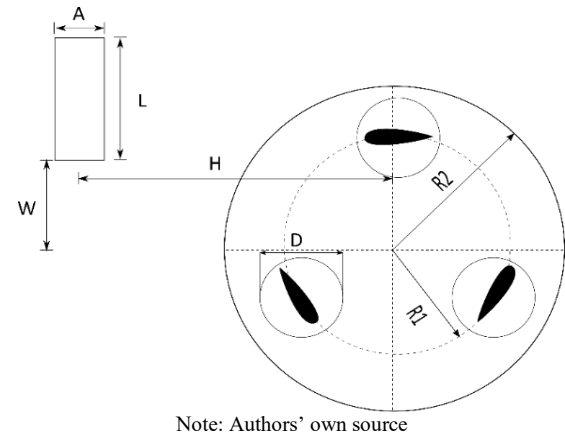

Note: Authors' own source

Figure 2. Main dimensions and configuration of control surfaces

Three specific cases were configured in the ANSYS R2024® Space Claim module: Case A serves as baseline case without blocking plate, while Case B and Case C have the

blocking plate at different distance from the rotor. Figure 1 shows the dimensions of the background grid as demonstrated by Munoz et al. [25] and the contour conditions which are the same for all the configured cases. Figure 2 illustrates the rotor and blocking plate design parameters.

Table 1 and Table 2 show the parameters considered, their symbology and the values taken by the DoE, according to the case, which was granted for the design of the rotor and blocking plate. Furthermore, plates were located according to Patel et al. [19] the positions are taken based on the diameter of the rotor. On the other hand, solidity was taken from the case of the previous study [25].

Table 1. General design parameters

Parameter	Symbol	Value [m]
Rotation radius	R1	0.450
Rotor radius	R2	0.850
Plate length	L	0.252
Plate width	A	0.100
Distance Y	W	0.300

Table 2. Design of experiments

Case	Factor: Solidity	Factor: Blocking Plate Position [m]
A	1.35, 1.79	No plate
B	1.35, 1.79	1.600
C	1.35, 1.79	0.665

2.3 Mesh generation and boundary conditions

The computational domains were performed in ICEM CFD. Structured grids were created with quadrilateral elements with separate domains to implement the overset method. Overset allows you to control the cells of each component and their respective movements. Figure 3 (a) shows the background grid which the blocking plate that corresponds to the stationary domain of the model, in the same way, it has refinement in the part where the rotating domain is located. Figure 3 (b) shows the rotor mesh which is configured as a rotary domain and Figure 3 (c) shows the discretization of the blade, it is configured as a rotary domain, but its movement is relative to the rotor.
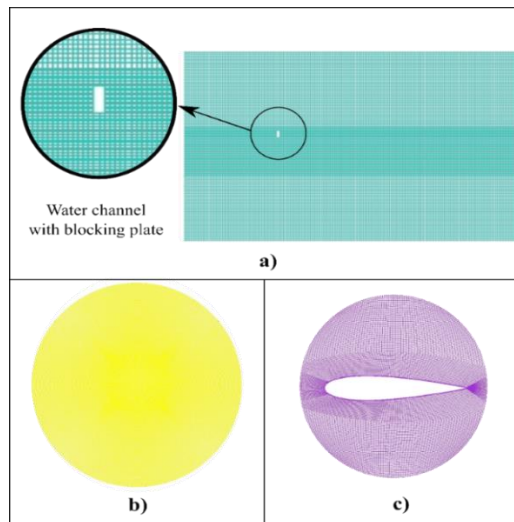
Note: Authors' own source

Figure 3. Discretization of control surfaces: a) Background grid mesh; b) Rotor mesh; c) Blade mesh

The metrics of the meshes made are illustrated in Table 3, which are in the acceptable ranges according to the ANSYS® user manual [13, 26, 27]. According to these references, the determinant must be greater than 0.3 and the aspect ratio must be between 1 and 300 depending on the type of simulation to guarantee an adequate mesh quality. These values guarantee the accuracy and stability of the results in the simulations carried out.

Table 3. Grid details and metrics

Components	Number of Elements	Min. Determinant 2 × 2 × 2	Max. Aspect Ratio
Standard grid	57882	1	2.180
Grid case B	47690	1	2.080
Grid case C	47668	1	9.830
Blade σ 1.35	16558	0.485	126
Blade σ 1.79	8990	0.995	123
Rotor	57321	0.948	3.070

The simulation was carried out in the ANSYS Fluent®, where the system was evaluated in the transient state with the standard turbulence model. According to the study of Munoz et al. [25], a convergence criterion of 1E-4 was configured. The total simulation time is 10 s with a time step of 0.005 s [26]. Table 4 summarizes the conditions configured in the simulation.

Table 4. Simulation parameters

Parameters	Value
Simulation types	Transitory
Turbulence model	$k - \varepsilon$ Realizable
Inlet velocity	1.620 m/s
Angular velocity	6.280 rad/s
Pressure	1 atm

k-ε Realizable turbulence models were used in this study because they correctly predict the behavior of turbines, and their computational performance compared to other turbulence models available in solvers. Moreover, the k-ε Realizable model improves upon the standard k-ε model by incorporating a more physically accurate formulation for turbulent viscosity and an improved dissipation rate equation, allowing it to better capture flow features such as boundary layer behavior and rotational flows [27-32]. The transport equations for k and ε in this turbulence model are given by Mohamed et al. [33]:

$$\frac{\partial}{\partial t}(\rho k) + \frac{\partial}{\partial x_i}(\rho k U_j) = \frac{\partial}{\partial x_i}\left[\left(\mu + \frac{\mu_t}{\sigma_k}\right)\frac{\partial \kappa}{\partial x_j}\right] + \cdots G_k + G_b - \rho\varepsilon - Y_M + S_k \quad (6)$$

$$\frac{\partial}{\partial t}(\rho\varepsilon) + \frac{\partial}{\partial x_j}(\rho\varepsilon U_j) = \frac{\partial}{\partial x_j}\left[\left(\mu + \frac{\mu_t}{\sigma_\varepsilon}\right)\frac{\partial \varepsilon}{\partial x_j}\right] + \cdots \rho C_1 S_t - \rho C_2 \frac{\varepsilon^2}{k + \sqrt{v\varepsilon}} + C_{1\varepsilon}\frac{\varepsilon^2}{\kappa}C_{3\varepsilon}G_b + S_t \quad (7)$$

where,

$$C_1 = max\left[0.43\frac{\eta}{\eta + 5}\right] \quad (8)$$

$$\eta = S\frac{k}{\varepsilon} \quad (9)$$

$$S = \sqrt{2S_{ij}S_{ij}} \qquad (10)$$

where, G_k is the turbulent kinetic energy due to the velocity gradient and G_b is the turbulent kinetic energy due to the buoyancy force. Y_M is also the contribution of pulsatile diffusion to compressible turbulence. The total dissipation rate σ_k and σ_ε are the turbulent Prandtl numbers k and ε, respectively, S_k and S_ε are user-defined source expressions.

3. RESULTS AND DISCUSSION

3.1 Statistical analysis

The results from the DoE-ANOVA are presented in this section. The data analysis was performed using Minitab software. The objective of the statistical analysis is to determine the optimal configuration that provides the best performance in the study. Twelve tests were carried out, and Table 5 shows the power coefficients C_p derived from each evaluated case.

Table 5. Numerical results obtained from fluent

Solidity [-]	Case	Average Torque [Nm]	Power [Watts]	C_p [-]	Efficiency [%]
1.35	A	112.381	705.756	0.37	37.00
	A	112.989	709.571	0.372	37.20
	B	124.227	780.146	0.409	40.90
	B	123.012	772.516	0.405	40.50
	C	130.606	820.203	0.43	43.00
	C	131.820	827.832	0.434	43.40
1.79	A	106.307	667.607	0.35	35.00
	A	107.825	677.144	0.355	35.50
	B	119.064	747.720	0.392	39.20
	B	116.937	734.367	0.385	38.50
	C	113.293	711.478	0.373	37.30
	C	115.419	724.830	0.38	38.00
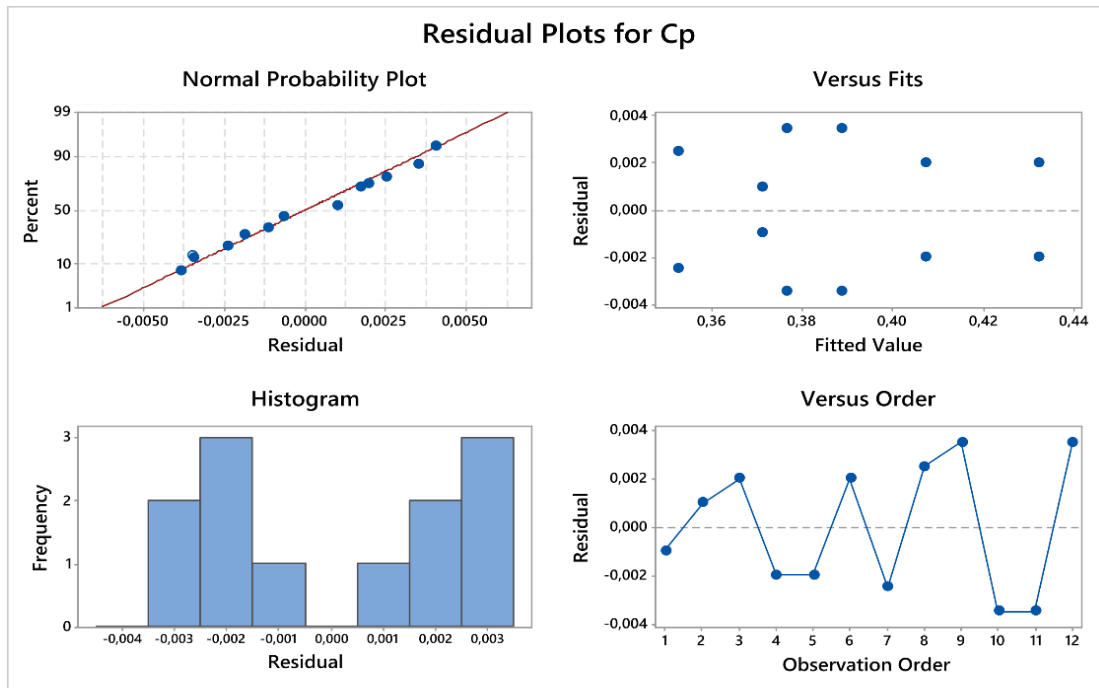
Note: Authors' own source

Figure 4. Residual plots of the quartic regression model predictions

Figure 4 presents the normal probability plot of residuals, demonstrating that the residuals follow a normal distribution. This confirms the assumption of normality for the evaluated model's residuals. Consequently, the ANOVA model can be appropriately applied, allowing for the continuation of statistical analysis.

The results of the ANOVA analysis are shown in Table 6. The F-value represents the ratio between the variance explained by each factor and the variance attributed to random error, while the P-value indicates whether that factor has a statistically significant effect on the Design of Experiment (DoE). When the P-value is below the established alpha level (0.05), the effect is significant, allowing the null hypothesis to be rejected. In this analysis, the results show that both solidity and the addition of blocking plates (Case) significantly influence the power coefficients, improving efficiency. Solidity, with a higher F-value, has the highest variance,

making it the most influential factor on system efficiency. This suggests that adjustments in solidity have a stronger impact on the power coefficient than variations in the blocking plates.

Table 6. Analysis of variance-ANOVA

Source	DF	Adj SS	Adj MS	F-Value	P-Value
Model	5	0.007709	0.001542	155.48	0.000
Linear	3	0.007069	0.002356	237.61	0.000
Solidity	1	0.003040	0.003040	306.56	0.000
Case	2	0.004029	0.002014	203.13	0.000
2-Way Interactions	2	0.000641	0.000320	32.30	0.001
Solidity*Case	2	0.000641	0.000320	32.30	0.001
Error	6	0.000060	0.000010	-	-
Total	11	0.007769	-	-	-

Note: DF, degree of freedom; Adj SS, adjusted sum of squares; Adj MS, adjusted mean square

Table 7. Model summary

S	R-sq	R-sq(adj)	R-sq(pred)
0.0031491	99.23%	98.60%	96.94%

Note: S, standard error; R-sq, the R-squared; R-sq adj adjusted R-squared

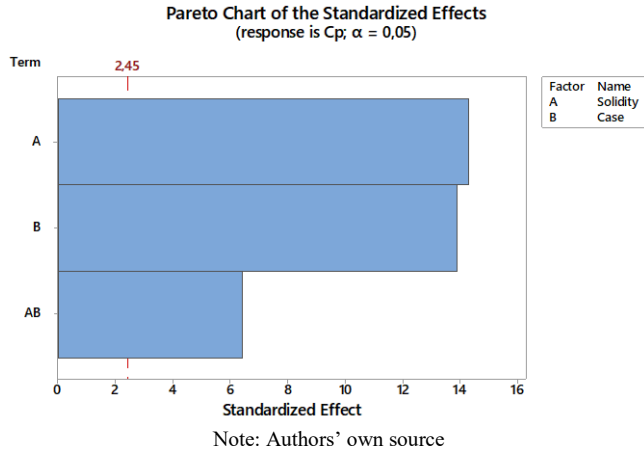

Note: Authors' own source

Figure 5. Pareto diagram

Table 7 presents a summary of the performance metrics of the model, explaining and predicting surface finish variability. In terms of fit and predictive ability the model reflects high accuracy and a solid ability to generalize new data.

The Pareto diagram shows the magnitude and importance of the effects individually and their respective combinations; likewise. the reference line (red line) indicates which effects are statistically significant [34]. Figure 5 shows that the factors A, B and AB interaction are statistically significant.

The objective is to determine what is the maximum power coefficient achieved. In this case analyzing the main effects in Figure 6 (a). When solidity increases from 1.35 to 1.79, a decrease in the average C_p value is observed, suggesting that higher solidity reduces efficiency, possibly due to increased aerodynamic drag. In contrast, C_p improves consistently from case A to C, indicating that case design positively influences performance, with case C being the most effective in maximizing efficiency. This is verified in Figure 6 (b) that shows the interaction graph between the factors and their different levels. The slopes of the lines in the interaction plot reveal how the impact of solidity varies from case to case. In case A, increasing solidity significantly decreases C_p, reflecting a negative interaction. On the other hand, cases B and C present smoother slopes, suggesting greater solidity to changes in solidity, especially in case C, where C_p remains high and stable, standing out as the most efficient option.

3.2 Numerical analysis

Figure 6 shows the variation of coefficient of moment C_m in a single blade for each case configured. Figure 7 (a) shows that with a solidity of 1.35. where the case with the best performance was case C. Similarly, Figure 7 (b) shows that with a solidity of 1.79, the case with the best performance is case B. Additionally, the behavior of this turbine exhibits a series of peaks or instabilities in the blades due to changes in the fluid associated with the blocking plate. These peaks represent fluctuations in the fluid when the solidity increases, indicating that solidity directly affects the behavior of the fluid and, consequently, the performance of the turbine. Furthermore, both rotors presented negative C_m, indicating the

lack of self-starting capacity of the HDHT. However, the rotor with a solidity of 1.35 has a self-starting capacity that is 45% better compared to the rotor with a solidity of 1.79.
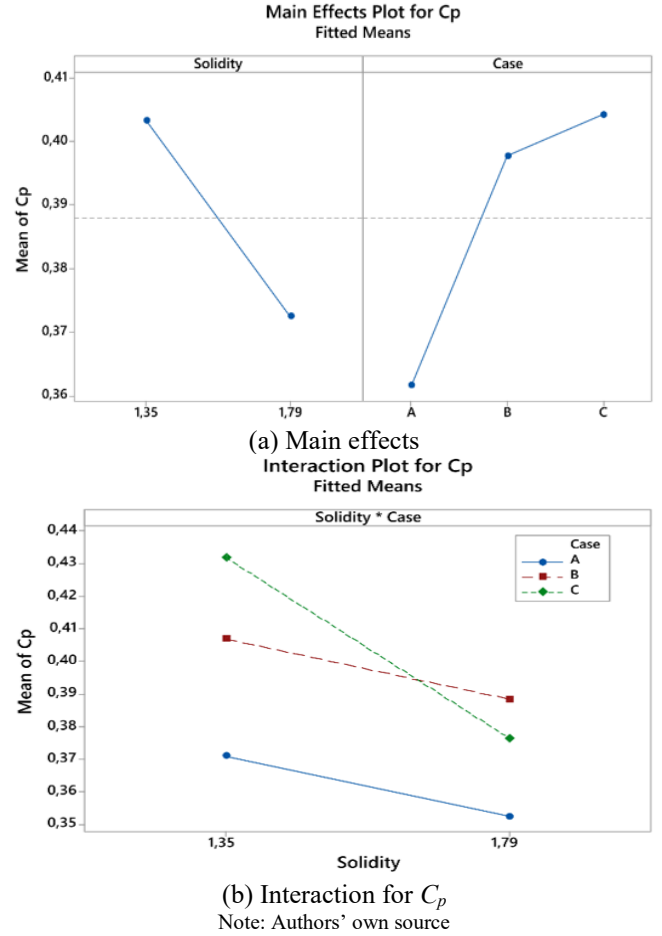

(a) Main effects

(b) Interaction for C_p

Note: Authors' own source

Figure 6. Fitted means for C_p

(a) solidity 1. 35

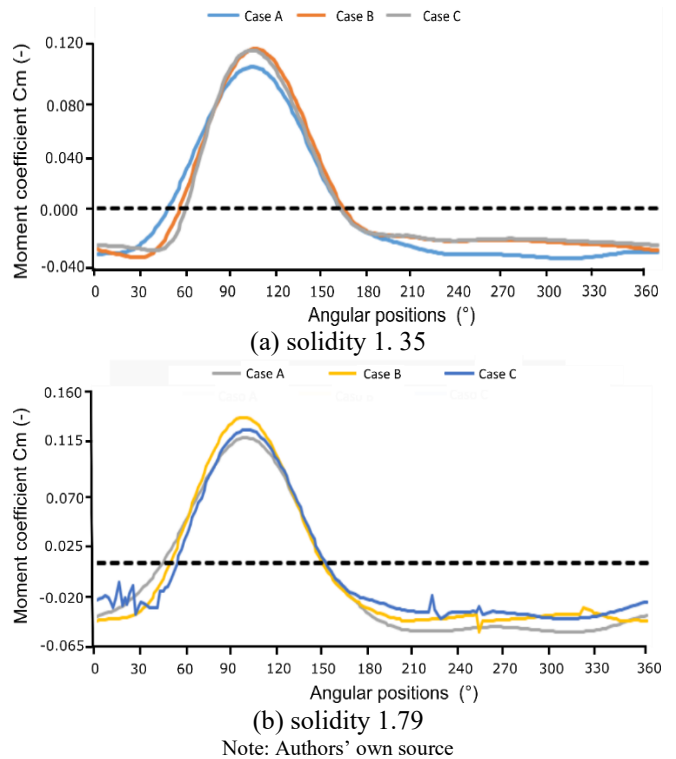(b) solidity 1.79

Note: Authors' own source

Figure 7. Variation moment coefficient in a single blade

Note: Authors own source

Table 8. Maximum and minimum moment coefficient

Solidity	Parameter	C_m Max	C_m Min	Improved Maximum C_m	Improved Minimum C_m
	Case A	0.106	-0.038	-	-
1.35	Case B	0.113	-0.034	6.091	12.155
	Case C	0.119	-0.032	10.592	19.906
	Case A	0.112	-0.063	-	-
1.79	Case B	0.130	-0.061	13.942	3.749
	Case C	0.124	-0.064	9.412	-0.592
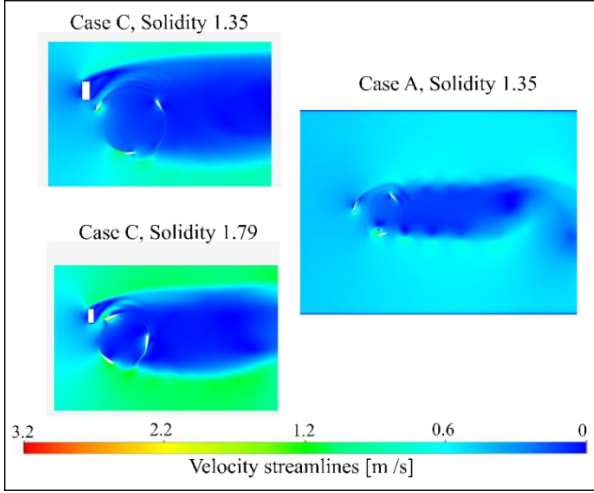
(a) Velocity for case C and case A
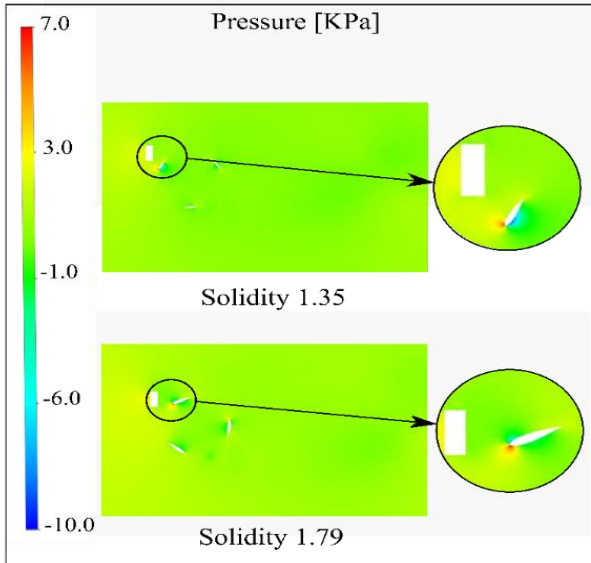
(b) Pressure for case C

Note: Authors' own source

Figure 8. CFD contour from Fluent

Table 8 shows the maximum and minimum values of C_m for configured cases. There is an improvement in the C_m and therefore in the efficiency of the turbine. However, not all cases show an improvement in the minimum C_m case C with solidity of 1.79 has an increase of 6% in its minimum C_m. The best cases for solidity 1.35 and 1.79 are case C and B respectively. with an improvement of approximately 10.6% and 13.9% with respect to case A.

The study by Patel et al. [19] is based on experimental tests, which provide results directly observed under real physical conditions, including factors such as fluid-structure interaction, material roughness, and secondary effects that are difficult to replicate numerically. On the other hand, the present study is based on numerical simulations using CFD, which can simplify or idealize certain physical aspects, such as boundary conditions or complex secondary effects, which partly explains the differences in the maximum C_p values.

Patel et al. [19] reported a maximum C_p of 0.36, while this study achieved a maximum C_p of 0.430 for the rotor configuration with the solidity of 1.79 configured with case B. These results are approximate; however, it suggests reviewing more positioning points for the plate as they do not match the parameterization suggested by the authors. Additionally, the differences may be due to the rotor under study not having all the dimensions of the turbine designed.

Figure 8 shows the velocity and pressure contours of case C and case A where the drop (blue color) and increase (red color) of rotor velocity and pressure are shown. Figure 8 (a) illustrates the velocity behavior of the water in case A and case C. It is observed how the flow changes due to the blocking plate, decreasing the velocity of the water in the upper quadrant and increasing it in the lower quadrant due to the turbulence projected by the accessory. Figure 8 (b) shows the pressure contour of case C, when solidity is 1.79, there is a bigger fluctuation in the pressures that may be due to having bigger solidity. It can be observed that higher velocities correspond to lower pressures, which is a normal behavior indicating that the simulation accurately represents the physical phenomena of the HDHTs.

4. CONCLUSIONS AND FUTURE WORK

Numerical study was carried out implementing statistical tools such as DoE-ANOVA. General factorial experimental design with two factors was configured with two and three factors. The study was conducted in ANSYS Fluent ® R2024, six configurations were simulated with a replica. The performance of each rotor was determined in terms of power and momentum coefficients, and it was concluded that:

Using Minitab® software, the statistical analysis of the experiment was carried out with two factors: solidity and blocking plate distance; the response variable analyzed was the power coefficient. From the statistical analysis it was found that both factors are significant to improve the power coefficient, likewise, it was found that the lowest solidity of 1.35 with case C (blocking plate at 0.665 m) is the best configuration. These data coincide with the numerical analysis carried out; on the other hand, the behavior of the total moment coefficient of the turbine was also analyzed and it was found that there is also a significant improvement in the minimum moment coefficient generated, which can directly impact the capacity of self-starting of the turbine and improving its cyclic behavior.

This research concludes that the DoE-ANOVA method is an effective strategy for understanding the effect of a variable on the behavior of the hydraulic and mechanical properties of H-Darrieus turbines. Where the use of statistical analysis along with simulation tools are shown as powerful tools to solve the turbine design problem, where the number of possible

solutions to be evaluated is reduced in order to find an adequate solution. These methods help ensure that simulation results are not only accurate but also reliable, by distinguishing between real physical effects and random noise or numerical errors.

In future studies, it is possible to consider a regression model that allows considering the variation of the TSR and the different positions and geometries of the locking plate, with the aim of minimizing the negative torque. It is also possible to develop a model that considers all the physical components of the HDHT in a three-dimensional model that allows the validation of the computational data in experimental configurations.

ACKNOWLEDGEMENTS

REFERENCES

[1] International Energy Agency (IEA). (2022). Renewables 2022 analysis and forecast to 2027. https://iea.blob.core.windows.net/assets/ada7af90-e280-46c4-a577-df2e4fb44254/Renewables2022.pdf.

[2] Ministerio de Minas y Energía. (2021). Transición energética: un legado para el presente y el futuro de Colombia. https://www.laimprentaeditores.com.

[3] Millán, J. (2015). Agua y energía. VII Foro Mundial del Agua, CAF, Caracas, http://scioteca.caf.com/handle/123456789/783.

[4] Dyner, I., Alvarez, C., Cherni, J. (2005). Energy contribution to sustainable rural livelihoods in developing countries: A system dynamics approach. In Proceedings of the 23rd International Conference of the System Dynamics Society, Boston, MA, USA, pp. 17-21.

[5] Balkhair, K.S., Rahman, K.U. (2017). Sustainable and economical small-scale and low-head hydropower generation: A promising alternative potential solution for energy generation at local and regional scale. Applied Energy, 188: 378-391. https://doi.org/10.1016/j.apenergy.2016.12.012

[6] Furukawa, A., Watanabe, S., Matsushita, D., Okuma, K. (2010). Development of ducted Darrieus turbine for low head hydropower utilization. Current Applied Physics, 10(2): S128-S132. https://doi.org/10.1016/j.cap.2009.11.005

[7] Perius, M.R., Carregaro, J.B. (2012). Pequenas centrais hidrelétricas como forma de redução de impactos ambientais e crises energéticas. Ensaios e Ciência C Biológicas Agrárias e da Saúde, 16(2): 135-150. https://doi.org/10.5585/EccoS.n27.3477

[8] Çetin, N.S., Yurdusev, M.A., Ata, R., Özdamar, A. (2005). Assessment of optimum tip speed ratio of wind turbines. Mathematical and Computational Applications, 10(1): 147-154. https://doi.org/10.3390/mca10010147

[9] Mon, E.E. (2019). Design of low head hydrokinetic turbine. International Journal of Trend in Scientific Research and Development (IJTSRD), 3(5): 2106-2109. https://doi.org/10.31142/ijtsrd27865

[10] Naeem, S.M. (2024). Structural and stress analysis of NACA0012 wing using SolidWorks. Mathematical Modelling of Engineering Problems, 11(8): 2181-2186. https://doi.org/10.18280/mmep.110820

[11] Mabrouk, I.B., El Hami, A. (2019). Effect of number of blades on the dynamic behavior of a Darrieus turbine geared transmission system. Mechanical Systems and Signal Processing, 121: 562-578. https://doi.org/10.1016/j.ymssp.2018.11.048

[12] Du, L., Ingram, G., Dominy, R.G. (2019). Experimental study of the effects of turbine solidity, blade profile, pitch angle, surface roughness, and aspect ratio on the H-Darrieus wind turbine self-starting and overall performance. Energy Science & Engineering, 7(6): 2421-2436. https://doi.org/10.1002/ese3.430

[13] Tobón, N.E.T., González, K.A.H., Hernandez, A.F.B., Del Rio, J.S., Zuluaga, D.A.H. (2020). Influencia de la solidez y el número de álabes en una turbina de eje vertical tipo H-darrieus. Revista Politécnica, 16(32): 9-18. https://doi.org/10.33571/rpolitec.v16n32a1

[14] Mohamed, M.H. (2013). Impacts of solidity and hybrid system in small wind turbines performance. Energy, 57: 495-504. https://doi.org/10.1016/j.energy.2013.06.004

[15] Hashem, I., Mohamed, M.H. (2018). Aerodynamic performance enhancements of H-rotor Darrieus wind turbine. Energy, 142: 531-545. https://doi.org/10.1016/j.energy.2017.10.036

[16] Patel, V., Eldho, T.I., Prabhu, S.V. (2017). Experimental investigations on Darrieus straight blade turbine for tidal current application and parametric optimization for hydro farm arrangement. International Journal of Marine Energy, 17: 110-135. https://doi.org/10.1016/j.ijome.2017.01.007

[17] Tunio, I.A., Shah, M.A., Hussain, T., Harijan, K., Mirjat, N.H., Memon, A.H. (2020). Investigation of duct augmented system effect on the overall performance of straight blade Darrieus hydrokinetic turbine. Renewable Energy, 153: 143-154. https://doi.org/10.1016/j.renene.2020.02.012

[18] Gosselin, R., Dumas, G., Boudreau, M. (2016). Parametric study of H-Darrieus vertical-axis turbines using CFD simulations. Journal of Renewable and Sustainable Energy, 8(5): 053301. https://doi.org/10.1063/1.4963240

[19] Patel, V., Eldho, T.I., Prabhu, S.V. (2019). Performance enhancement of a Darrieus hydrokinetic turbine with the blocking of a specific flow region for optimum use of hydropower. Renewable Energy, 135: 1144-1156. https://doi.org/10.1016/j.renene.2018.12.074

[20] Rueda-Bayona, J.G., Paez, N., Cabello Eras, J.J., Sagastume Gutierrez, A. (2022). DOE-ANOVA to optimize hydrokinetic turbines for low velocity conditions. Mathematical Modelling of Engineering Problems, 9(4): 979-988. https://doi.org/10.18280/mmep.090415

[21] Favrel, A., Lee, N.J., Irie, T., Miyagawa, K. (2021). Design of experiments applied to Francis turbine draft tube to minimize pressure pulsations and energy losses in off-design conditions. Energies, 14(13): 3894. https://doi.org/10.3390/en14133894

[22] Hatami, M., Cuijpers, M.C., Boot, M.D. (2015). Experimental optimization of the vanes geometry for a variable geometry turbocharger (VGT) using a Design of Experiment (DoE) approach. Energy Conversion and

Management, 106: 1057-1070. https://doi.org/10.1016/j.enconman.2015.10.040

[23] Huang, S.R., Ma, Y.H., Chen, C.F., Seki, K., Aso, T. (2014). Theoretical and conditional monitoring of a small three-bladed vertical-axis micro-hydro turbine. Energy conversion and Management, 86: 727-734. https://doi.org/10.1016/J.ENCONMAN.2014.05.098

[24] Alam, M.J., Iqbal, M.T. (2009). Design and development of hybrid vertical axis turbine. In 2009 Canadian Conference on Electrical and Computer Engineering, St. John's, NL, Canada, pp. 1178-1183. https://doi.org/10.1109/CCECE.2009.5090311

[25] Munoz, A.G., Hincapié Zuluaga, D.A., Rio, J.S.D., Rodriguez-Cabal, M.A., Torres-Lopez, E. (2023). Numerical comparison and efficiency analysis of three vertical axis turbine of H-Darrieus type. EUREKA: Physics and Engineering, 2: 28-39. https://doi.org/10.21303/2461-4262.2023.002593

[26] Lucas, D., Tomiyama, A. (2011). On the role of the lateral lift force in poly-dispersed bubbly flows. International Journal of Multiphase Flow, 37(9): 1178-1190.
https://doi.org/10.1016/j.ijmultiphaseflow.2011.05.009

[27] Ceballos, Y.C., Valencia, M.C., Zuluaga, D.H., Del Rio, J.S., García, S.V. (2017). Influence of the number of blades in the power generated by a Michell Banki Turbine. International Journal of Renewable Energy Research, 7(4): 1989-1997.

[28] Wang, S., Ingham, D.B., Ma, L., Pourkashanian, M., Tao, Z. (2012). Turbulence modeling of deep dynamic stall at relatively low Reynolds number. Journal of Fluids and Structures, 33: 191-209. https://doi.org/10.1016/j.jfluidstructs.2012.04.011

[29] Almohammadi, K.M., Ingham, D.B., Ma, L., Pourkashan, M. (2013). Computational fluid dynamics (CFD) mesh independency techniques for a straight blade vertical axis wind turbine. Energy, 58: 483-493. https://doi.org/10.1016/j.energy.2013.06.012

[30] Lanzafame, R., Mauro, S., Messina, M. (2014). 2D CFD modeling of H-Darrieus wind turbines using a transition turbulence model. Energy Procedia, 45: 131-140. https://doi.org/10.1016/j.egypro.2014.01.015

[31] Daróczy, L., Janiga, G., Petrasch, K., Webner, M., Thévenin, D. (2015). Comparative analysis of turbulence models for the aerodynamic simulation of H-Darrieus rotors. Energy, 90: 680-690. https://doi.org/10.1016/j.energy.2015.07.102

[32] Marsh, P., Ranmuthugala, D., Penesis, I., Thomas, G. (2017). The influence of turbulence model and two and three-dimensional domain selection on the simulated performance characteristics of vertical axis tidal turbines. Renewable Energy, 105: 106-116. https://doi.org/10.1016/j.renene.2016.11.063

[33] Mohamed, M.H., Ali, A.M., Hafiz, A.A. (2015). CFD analysis for H-rotor Darrieus turbine as a low speed wind energy converter. Engineering Science and Technology, an International Journal, 18(1): 1-13. https://doi.org/10.1016/j.jestch.2014.08.002

[34] Soporte técnico de Minitab 19–Minitab. https://support.minitab.com/es-mx/minitab/19/.